

Alerts in High-resolution TEM characterization of perovskite material

Yu-Hao Deng^{1*}

¹ Academy for Advanced Interdisciplinary Studies, Peking University, Beijing, China

* Correspondence should be addressed to yuhaodeng@pku.edu.cn

Abstract

High-resolution TEM (HRTEM) is a powerful tool for structure characterization. However, MAPbI_3 perovskite is highly sensitive to electron beams and easily decompose into PbI_2 . Universal mistakes that PbI_2 is incorrectly labeled as perovskite are widely exist in HRTEM characterizations, which negatively affect the development of perovskite research field. Here errors in MAPbI_3 perovskite calibration are statisticed and identified based on corresponding electron diffraction (ED) simulations. Corrected material phases, ED patterns of original PbI_2 and obvious crystallographic parameters are also presented. This approach paves the way to avoid misleadings in HRTEM characterization of perovskite and other electron beam-sensitive materials in the future.

Introduction

High-resolution transmission electron microscopy (HRTEM) is a very powerful characterization tool and has been extensively and successfully used for analyzing crystal structures on an atomic resolution scale^[1]. Recently, halide perovskites have achieved substantial success in various optoelectronic devices owing to their solution-based growth method and remarkable physical properties^[2-5]. However, MAPbI_3 perovskite is very sensitive to electron beam irradiation. As a rough estimation, MAPbI_3 begins to decompose into PbI_2 under $150 \text{ e}\text{\AA}^{-2}$ total dose irradiation^[6, 7]. Figure 1 shows the MAPbI_3 degradation process under electron beam irradiation. Tetragonal perovskite decomposes into hexagonal lead iodide by the escape of methylamine and hydrogen iodide molecules.

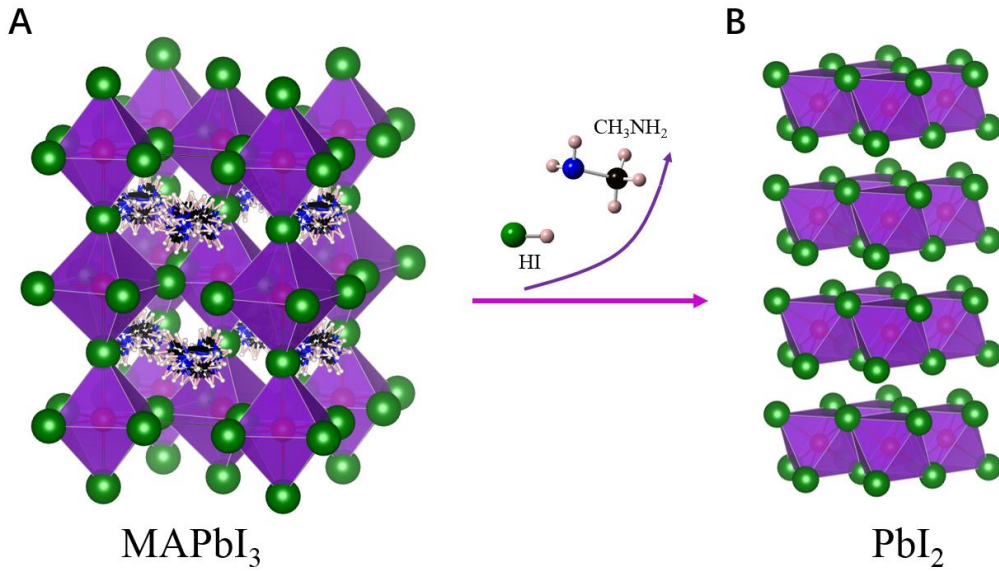


Fig. 1. MAPbI₃ degradation under electron beam irradiation. Tetragonal perovskite (**A**) decomposes into hexagonal lead iodide (**B**), followed by the escape of methylamine and hydrogen iodide molecules. Here, colors represent the following: green, iodine; red, lead; black, carbon; blue, nitrogen; pink, hydrogen.

Results and discussion

General phase calibration method of HRTEM data is to compare a group of interplanar spacings and angles. This method is easy to ignore the absent crystal planes, leading to mistaken calibration results. For instance, the lead iodide is generally labeled as perovskite^[8]. Figure 2 shows simulated ED patterns of MAPbI₃ and PbI₂ along different axis zones. These crystal planes are often confused in perovskite calibrations. Figure 2A is the ED pattern of MAPbI₃ along [110] axis zone. (1̄10), (002) crystal planes are existing in a perfect tetragonal perovskite, but they are missing in HRTEM characterizations in previous research papers. The absence of crystal planes indicates that the material is no longer MAPbI₃ perovskite, but other phases and structures. Figure 2B shows the simulated ED patterns of PbI₂ along [4̄41] axis zone. (014), (1̄04) crystal planes of PbI₂ have the very closed interplanar spacing and angle with (2̄20), (004) crystal planes of MAPbI₃. Actually MAPbI₃ has been damaged into PbI₂ phase by electron beams and neglect of the lack of crystal planes results in the mischaracterization. Similarly, Figure 2C-H are ED patterns of MAPbI₃ along [101] and PbI₂ along [8101], MAPbI₃ along [2̄01] and PbI₂ along [8̄81], MAPbI₃ along [1̄20] and PbI₂ along [4̄11] respectively.

Diffraction spots circled in red are missing crystal planes that were neglected in HRTEM characterizations. Moreover, these neglected planes are all present in X-ray diffraction (XRD) of MAPbI_3 [9-11].

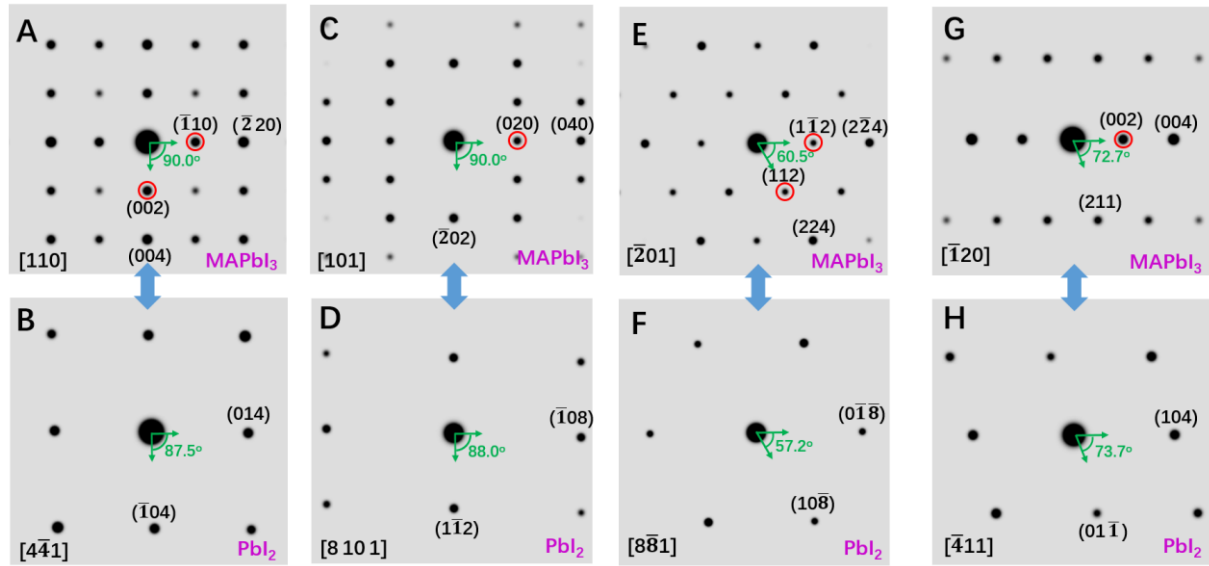


Fig. 2. Simulated electron diffraction (ED) patterns of tetragonal MAPbI_3 and hexagonal PbI_2 . (A) MAPbI_3 along $[110]$ axis zone. **(B)** PbI_2 along $[4\bar{4}1]$ axis zone. **(C)** MAPbI_3 along $[101]$ axis zone. **(D)** PbI_2 along $[8\ 10\ 1]$ axis zone. **(E)** MAPbI_3 along $[\bar{2}01]$ axis zone. **(F)** PbI_2 along $[8\bar{8}1]$ axis zone. **(G)** MAPbI_3 along $[\bar{1}20]$ axis zone. **(H)** PbI_2 along $[\bar{4}11]$ axis zone. Crystal planes marked in red circle are often missing in published articles.

The mischaracterizations have negatively affected the development of perovskite scientific research field. Statistically, these errors occur in the following fields: phase identification and structure determination [12], grain, nanowire and microwire orientation [13-17], morphology analysis and shape control of nanocrystals [18], growth direction of perovskite materials [19], degradation process and kinetics of perovskite [20], phase transition research in perovskite [21] and ion migration characterization in photoelectric devices [22]. Not only in the field of single MAPbI_3 material system, misleading information also occurs in the research field of heterostructure materials. Such as lattice matching and kinetic study in epitaxial growth of perovskite films on 2D material [23], PbS quantum dots in perovskite material [24, 25] and lattice anchoring stabilizes perovskite research [26]. To make the comparisons and corrections clearer, Table 1 shows the detailed parameters of the MAPbI_3 and PbI_2 along different axis zone, missing crystal planes have been marked in brown. Even remarkably, the $[110]$ and $[001]$ zone axis are equivalent in tetragonal MAPbI_3 perovskite.

Table 1. Detailed crystallographic parameters of MAPbI₃ and PbI₂.

Material and zone axis	Characteristic crystal planes	Interplanar spacing	Interplanar Angle	References
MAPbI₃ [110]	($\bar{1}10$), ($\bar{2}20$) (002), (004)	d($\bar{1}10$)= 6.2 Å. d($\bar{2}20$)= 3.1 Å. d(002)= 6.3 Å. d(004) =3.2 Å.	<($\bar{1}10$), (002)> = <($\bar{2}20$), (004)> =90.0°	12-23
PbI₂ [4̄1]	(014) ($\bar{1}04$)	d(014)= 3.2 Å. d($\bar{1}04$) =3.2 Å.	<(014), ($\bar{1}04$)> =87.5°	_____
MAPbI₃ [101]	(020), (040) ($\bar{2}02$)	d(020)= 4.4 Å. d(040)= 2.2 Å. d($\bar{2}02$)= 3.6 Å.	<(020), ($\bar{2}02$)> = <(040), ($\bar{2}02$)> =90.0°	27, 28
PbI₂ [8 10 1]	($\bar{1}08$) (1 $\bar{1}2$)	d($\bar{1}08$)= 2.2 Å. d(1 $\bar{1}2$)= 3.7 Å.	<($\bar{1}08$), (1 $\bar{1}2$)> =88.0°	_____
MAPbI₃ [$\bar{2}01$]	(1 $\bar{1}2$), (2 $\bar{2}4$) (112), (224)	d(1 $\bar{1}2$)= 4.4 Å. d(2 $\bar{2}4$)= 2.2 Å. d(112)= 4.4 Å. d(224)= 2.2 Å.	<(1 $\bar{1}2$), (112)> = <(2 $\bar{2}4$), (224)> =60.5°	14, 24-26
PbI₂ [8̄81]	(0 $\bar{1}8$) (10 $\bar{8}$)	d(0 $\bar{1}8$)= 2.2 Å. d(10 $\bar{8}$)= 2.2 Å.	<(0 $\bar{1}8$), (10 $\bar{8}$)> =57.2°	_____
MAPbI₃ [$\bar{1}20$]	(002), (004) (211)	d(002)= 6.3 Å. d(004) =3.2 Å. d(211)= 3.8 Å.	<(002), (211)> = <(004), (211)> =72.7°	29-32
PbI₂ [4̄11]	(104) (01 $\bar{1}$)	d(104)= 3.2 Å. d(01 $\bar{1}$)= 3.9 Å.	<(104), (01 $\bar{1}$)> =73.7°	_____

Conclusions

Above statistics and corrections are very helpful for researchers to avoid mistakes in perovskite research field. Others that incorrectly label metallic lead as perovskite can also be identified and corrected using the same method^[33]. Lessons learned from the mistakes alert us it is unreliable to calibrate material phase only by measuring interplanar spacings and angles. We also need to refer simulated ED or XRD specimen data to ensure the crystal planes are complete. In addition, low dose irradiation^[6, 34, 35] and low temperature^[7, 36] can reduce the damage of electron beam irradiation to perovskite, and may help us get the real structure of perovskite

materials. This work provides a sober-minded brain for further characterization in organic-inorganic hybrid perovskite and other electron beam-sensitive materials.

Methods

The Electron diffraction (ED) simulations of MAPbI_3 and PbI_2 were obtained using CrystalMaker Software. Corresponding crystal structures cif files were downloaded from Crystallography Open Database (COD) website. COD IDs of MAPbI_3 and PbI_2 are 4124388 and 9009141 respectively. MAPbI_3 is $I4/mcm$ space group with tetragonal structure, cell parameters: $a=b=8.839\text{\AA}$, $c=12.695\text{\AA}$; $\alpha=\beta=\gamma=90^\circ$. PbI_2 is $P-3m1$ space group with hexagonal structure, cell parameters: $a=b=4.555\text{\AA}$, $c=20.937\text{\AA}$; $\alpha=\beta=90^\circ$, $\gamma=120^\circ$.

Data availability

All data are available from the corresponding author(s) upon reasonable request.

References

- [1]. Jia C L, Lentzen M, Urban K. Atomic-resolution imaging of oxygen in perovskite ceramics[J]. *Science*, 2003, 299(5608): 870-873.
- [2]. <https://www.nrel.gov/pv/cell-efficiency.html>, Best Research-Cell Efficiencies, National Renewable Energy Laboratory, accessed: 7, 2020.
- [3]. Lin K, Xing J, Quan L N, et al. Perovskite light-emitting diodes with external quantum efficiency exceeding 20 per cent[J]. *Nature*, 2018, 562(7726): 245-248.
- [4]. Yang Z, Deng Y, Zhang X, et al. High-Performance Single-Crystalline Perovskite Thin-Film Photodetector[J]. *Advanced Materials*, 2018, 30(8): 1704333.
- [5]. Zhu H, Fu Y, Meng F, et al. Lead halide perovskite nanowire lasers with low lasing thresholds and high quality factors[J]. *Nature materials*, 2015, 14(6): 636-642.
- [6]. Chen S, Zhang X, Zhao J, et al. Atomic scale insights into structure instability and decomposition pathway of methylammonium lead iodide perovskite[J]. *Nature communications*, 2018, 9(1): 1-8.
- [7]. Li Y, Zhou W, Li Y, et al. Unravelling degradation mechanisms and atomic structure of organic-inorganic halide perovskites by cryo-EM[J]. *Joule*, 2019, 3(11): 2854-2866.
- [8]. Chen S, Gao P. Challenges, myths, and opportunities of electron microscopy on halide perovskites[J]. *Journal of Applied Physics*, 2020, 128(1): 010901.
- [9]. Dong Q, Fang Y, Shao Y, et al. Electron-hole diffusion lengths $> 175 \mu\text{m}$ in solution-grown $\text{CH}_3\text{NH}_3\text{PbI}_3$

single crystals[J]. *Science*, 2015, 347(6225): 967-970.

[10]. Mei A, Li X, Liu L, et al. A hole-conductor-free, fully printable mesoscopic perovskite solar cell with high stability[J]. *Science*, 2014, 345(6194): 295-298.

[11]. Shi D, Adinolfi V, Comin R, et al. Low trap-state density and long carrier diffusion in organolead trihalide perovskite single crystals[J]. *Science*, 2015, 347(6221): 519-522.

[12]. Yang M, Zhou Y, Zeng Y, et al. Square-centimeter solution-processed planar $\text{CH}_3\text{NH}_3\text{PbI}_3$ perovskite solar cells with efficiency exceeding 15%[J]. *Advanced Materials*, 2015, 27(41): 6363-6370.

[13]. Xiao M, Huang F, Huang W, et al. A fast deposition-crystallization procedure for highly efficient lead iodide perovskite thin-film solar cells[J]. *Angewandte Chemie International Edition*, 2014, 53(37): 9898-9903.

[14]. Yang B, Dyck O, Poplawsky J, et al. Controllable Growth of Perovskite Films by Room-Temperature Air Exposure for Efficient Planar Heterojunction Photovoltaic Cells[J]. *Angewandte Chemie International Edition*, 2015, 54(49): 14862-14865.

[15]. Son D Y, Lee J W, Choi Y J, et al. Self-formed grain boundary healing layer for highly efficient $\text{CH}_3\text{NH}_3\text{PbI}_3$ perovskite solar cells[J]. *Nature Energy*, 2016, 1(7): 1-8.

[16]. Zhu H, Fu Y, Meng F, et al. Lead halide perovskite nanowire lasers with low lasing thresholds and high quality factors[J]. *Nature materials*, 2015, 14(6): 636-642.

[17]. Li S, Li Y, Shi Z, et al. Fabrication of morphology-controlled and highly-crystallized perovskite microwires for long-term stable photodetectors[J]. *Solar Energy Materials and Solar Cells*, 2019, 191: 275-282.

[18]. Zhu F, Men L, Guo Y, et al. Shape evolution and single particle luminescence of organometal halide perovskite nanocrystals[J]. *ACS nano*, 2015, 9(3): 2948-2959.

[19]. Gao L, Zeng K, Guo J, et al. Passivated single-crystalline $\text{CH}_3\text{NH}_3\text{PbI}_3$ nanowire photodetector with high detectivity and polarization sensitivity[J]. *Nano letters*, 2016, 16(12): 7446-7454.

[20]. Fan Z, Xiao H, Wang Y, et al. Layer-by-layer degradation of methylammonium lead tri-iodide perovskite microplates[J]. *Joule*, 2017, 1(3): 548-562.

[21]. Li D, Wang G, Cheng H C, et al. Size-dependent phase transition in methylammonium lead iodide perovskite microplate crystals[J]. *Nature communications*, 2016, 7(1): 1-8.

[22]. Kim S, Bae S, Lee S W, et al. Relationship between ion migration and interfacial degradation of $\text{CH}_3\text{NH}_3\text{PbI}_3$ perovskite solar cells under thermal conditions[J]. *Scientific reports*, 2017, 7(1): 1-9.

[23]. Tang G, You P, Tai Q, et al. Solution-Phase Epitaxial Growth of Perovskite Films on 2D Material Flakes for High-Performance Solar Cells[J]. *Advanced Materials*, 2019, 31(24): 1807689.

[24]. Ning Z, Gong X, Comin R, et al. Quantum-dot-in-perovskite solids[J]. *Nature*, 2015, 523(7560): 324-328.

[25]. Gong X, Yang Z, Walters G, et al. Highly efficient quantum dot near-infrared light-emitting diodes[J]. *Nature Photonics*, 2016, 10(4): 253-257.

[26]. Liu M, Chen Y, Tan C S, et al. Lattice anchoring stabilizes solution-processed semiconductors[J]. *Nature*, 2019, 570(7759): 96-101.

[27]. Kim T W, Uchida S, Matsushita T, et al. Self-Organized Superlattice and Phase Coexistence inside Thin

Film Organometal Halide Perovskite[J]. *Advanced Materials*, 2018, 30(8): 1705230.

[28]. Wang G, Li D, Cheng H C, et al. Wafer-scale growth of large arrays of perovskite microplate crystals for functional electronics and optoelectronics[J]. *Science advances*, 2015, 1(9): e1500613.

[29]. Niu L, Liu X, Cong C, et al. Controlled synthesis of organic/inorganic Van der waals solid for tunable light-matter interactions[J]. *Advanced materials*, 2015, 27(47): 7800-7808.

[30]. Liu X, Niu L, Wu C, et al. Periodic Organic-Inorganic Halide Perovskite Microplatelet Arrays on Silicon Substrates for Room-Temperature Lasing[J]. *Advanced Science*, 2016, 3(11): 1600137.

[31]. Kim T W, Shibayama N, Cojocaru L, et al. Real-time *in situ* observation of microstructural change in organometal halide perovskite induced by thermal degradation[J]. *Advanced Functional Materials*, 2018, 28(42): 1804039.

[32]. Zhao J, Kong G, Chen S, et al. Single crystalline $\text{CH}_3\text{NH}_3\text{PbI}_3$ self-grown on FTO/TiO₂ substrate for high efficiency perovskite solar cells[J]. *Science Bulletin*, 2017, 62(17).

[33]. Wang T, Zhang H, Hou S, et al. Facile synthesis of methylammonium lead iodide perovskite with controllable morphologies with enhanced luminescence performance[J]. *Nanomaterials*, 2019, 9(12): 1660.

[34]. Zhang D, Zhu Y, Liu L, et al. Atomic-resolution transmission electron microscopy of electron beam-sensitive crystalline materials[J]. *Science*, 2018, 359(6376): 675-679.

[35]. Chen S, Zhang Y, Zhao J, et al. Transmission electron microscopy of organic-inorganic hybrid perovskites: myths and truths[J]. *Science Bulletin*, 2020.

[36]. Zhu Y, Gui Z, Wang Q, et al. Direct atomic scale characterization of the surface structure and planar defects in the organic-inorganic hybrid $\text{CH}_3\text{NH}_3\text{PbI}_3$ by Cryo-TEM[J]. *Nano Energy*, 2020: 104820.